

A Multiyear Regional Climate Hindcast for the Western United States Using the Mesoscale Atmospheric Simulation Model

JINWON KIM

University of California, Los Angeles, Los Angeles, California

JUNG-EUN LEE

University of California, Berkeley, Berkeley, California

(Manuscript received 14 February 2002, in final form 20 November 2002)

ABSTRACT

In preparation for studying the effects of increased CO₂ on the hydrologic cycle in the western United States, an 8-yr hindcast was performed using a regional climate model (RCM) driven by the large-scale forcing from the NCEP–NCAR reanalysis. The simulated precipitation characteristics agree well with observations, especially in the winter. The simulated precipitation compares with rain gauge data at similar accuracy as the NCEP reanalysis, but the RCM-generated precipitation is more accurate than the reanalysis data at the scales of individual basins. Important characteristics of the hydrologic cycle of the region, such as seasonal snowfall, frequency of heavy and extreme daily precipitation events, and interannual variations of precipitation associated with the North American monsoon are also well represented in the hindcast. Compared to the Climate Research Unit, University of East Anglia (CRU), analysis, the simulated low-level air temperatures show cold biases except in summer. The temperature biases are difficult to quantify, however, due to suspected warm biases in the CRU data. The RCM overestimates surface insolation and outgoing longwave radiation at the top of the atmosphere (OLR–TOA). The errors in the simulated radiation are smaller over the land than the ocean. Both simulated and observed OLR–TOA suggest strong influence of low-level temperatures on the seasonal variations of OLR–TOA in the region. The results suggest that the RCM employed in this study possesses reasonable skill for studying regional climate change signals in the western United States.

1. Introduction

The impacts of the climate change associated with increased atmospheric CO₂ on a regional hydrologic cycle are an important concern. The hydrologic cycle of the western United States is characterized by large interseasonal variations in precipitation, as well as strong orographic effects in determining the spatial distribution of precipitation, snow budget, and streamflow (e.g., Goodridge 1994; Cayan et al. 1993; Kim 1997). Kim (2001) and Kim et al. (2002) showed that moderate changes in the large-scale moisture and low-level temperature induced by increased CO₂ may affect important features of the hydrologic cycles of the region significantly.

Assessing the impacts of climate change on human society, water resources, and the natural environment requires an accurate downscaling system to obtain regional-scale data for driving impact assessment models

from large-scale climate data. Dynamical downscaling uses a nested modeling system in which a fine-resolution, limited-area model is nested within the large-scale data from general circulation model (GCM) outputs. It requires a large amount of computational resources, but can generate physically and dynamically consistent regional-scale data. Recent progress in regional climate models (RCMs) and computers has made it possible to simulate long-term regional climate data with detailed physical processes involved in the feedback among the atmosphere, hydrosphere, lithosphere, and biosphere (e.g., Dickinson et al. 1989; Giorgi and Bates 1989; Kim and Soong 1996; Hong and Leetmaa 1999). In conjunction with assessment models, RCMs are widely used to study regional climate variations and impacts on various sectors such as water resources and agriculture (e.g., Mearns et al. 1996; Kim et al. 1998a,b). The time-scales at which RCMs are used for climate simulations usually range from a season to decades. In addition to investigations of regional climate characteristics (e.g., Barnston et al. 1999), seasonal simulations have become important for assessing water resources (e.g., Kim 1997; Kim et al. 1998a,b) and for seasonal predictions (Kim et al. 2000). Multiyear regional simulations have been

Corresponding author address: Dr. Jinwon Kim, Department of Atmospheric Sciences, University of California, Los Angeles, 405 Hilgard Ave., Los Angeles, CA 90095-1565.
E-mail: jkim@atmos.ucla.edu

used to project the effects of global climate change in particular regions (e.g., Giorgi et al. 1994, 1997; Kim 2001; Kim et al. 2002).

The accuracy of simulated regional climate data is crucial for reducing uncertainties in assessing impacts of climate variations and change. For example, precipitation affects streamflow, water resources, ecosystems, and industries such as agriculture. Snow is an important part of the hydrologic cycle in the western United States, especially in high-elevation areas. Snow budget plays a crucial role in the water supply from late spring to early fall (Cayan et al. 1993) as well. As with GCM simulations, climate data generated by RCMs are not free of errors due to model biases, a lack of land surface information (e.g., vegetation characteristics, soil texture), and inaccurate forcing data. Performance of an RCM varies for different domain size, spatial resolution, and season. Hence, an essential exercise prior to applying dynamically downscaled climate change scenarios for impact assessment is a rigorous evaluation of the RCMs to be employed in the regional assessment studies against observations and assimilations.

We evaluate precipitation characteristics, snow budget, low-level temperatures, radiation fields, and upper-air temperature and geopotential fields from an 8-yr regional climate hindcast for the western United States against available observations and analyses. Descriptions of the RCM employed in this study and experimental design are presented next. Evaluations of the hindcast results are subsequently presented.

2. Model and experimental descriptions

Details of the RCM used in this study, the Mesoscale Atmospheric Simulation (MAS), have been presented by Kim and Soong (1996) and Soong and Kim (1996). The MAS is a primitive equation, limited-area atmospheric model that uses the σ coordinate in the vertical. It is the dynamical downscaling part of the Regional Climate System Model (RCSM; Kim et al. 1998a,b), in which a suite of climate impact assessment models are linked to the downscaled data. In this study, we employ an 18-layer version of the MAS with a $36 \times 36 \text{ km}^2$ resolution grid covering the western United States (Fig. 1a).

Dependent variables of the MAS are staggered on the Arakawa C grid in the horizontal, and on the Lorenz grid in the vertical. The advection equation is solved using the third-order-accurate finite-difference scheme of Takacs (1985), which is characterized with minimal phase errors. A four-class version of the cloud microphysics scheme of Cho et al. (1989) and the Simplified Arakawa-Schubert scheme (SAS; Pan and Wu 1995; Hong and Pan 1998) are used to compute grid-scale and convective precipitation, respectively. Solar and terrestrial radiative transfer processes are computed using the formulations of Harshvardhan et al. (1987), after the effects of ice- (Stephens 1978) and water-phase (Starr

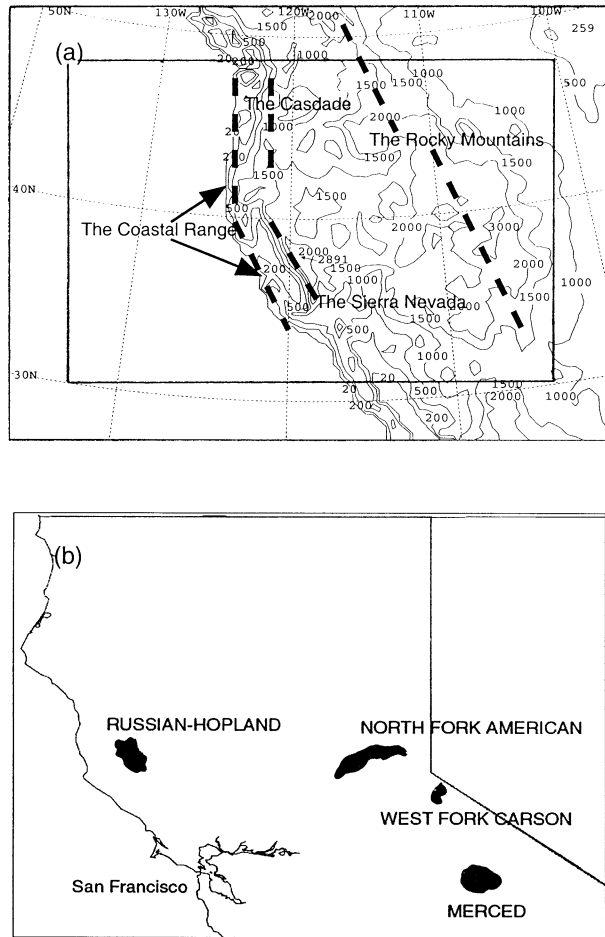


FIG. 1. (a) The RCM terrain at a 36-km horizontal resolution on a Lambert conformal projection used in the hindcast. Dashed lines indicate the locations of major mountain ranges; (b) indicates locations of the four California river basins. The area between the inner and outer boxes in (a) is the lateral boundary nudging zone. The mean elevation of each basin are: Hopland (458 m), North Fork American River (1304 m), West Fork Carson River (2456 m), and Merced River (2581 m).

and Cox 1985) cloud particles are added. Vertical turbulent mixing is computed using the bulk aerodynamic scheme of Deardorff (1978) at the surface, and the K-theory within the model atmosphere, respectively. The eddy diffusivities are computed using the local scheme by Louis et al. (1982) with the asymptotic mixing length of Kim and Mahrt (1992).

A two-layer version of the Soil-Plant-Snow (SPS) model (Kim and Ek 1995) is coupled with the MAS to compute the land surface processes. The SPS predicts the volumetric soil moisture content (SMC), soil temperature, canopy water content, and water-equivalent snow depth. The temperature and specific humidity at the atmosphere-land interface are calculated by solving a nonlinear form of the surface energy balance equation. More details of the SPS and its verifications are available in Mahrt and Pan (1984), Pan and Mahrt (1987),

Kim and Ek (1995), and Chang et al. (1999). In this study, the thickness of the upper and lower soil layers are set to 5 and 195 cm, respectively.

The regional climate simulation presented later covers the 8-yr period from January 1988 to December 1995. The initial conditions at 0000 UTC 1 January 1988, and the time-dependent boundary conditions including the sea surface temperature (SST) for the next 8 yr are obtained from the National Centers for Environmental Prediction–National Center for Atmospheric Research (NCEP–NCAR) reanalysis at a 2.5° resolution (Kalnay et al. 1996, reanalysis hereafter). Lateral boundary conditions are updated at 12-h intervals during the simulation using the Davies (1976) nudging scheme.

The initial soil variables, volumetric soil moisture content and soil temperature, are obtained from the corresponding reanalysis data. The reanalysis soil variables can be used in this study without major modifications, as the land surface variables in the reanalysis model are defined in the same way as they are in the SPS. First, soil data in the reanalysis are horizontally interpolated onto the regional model grid. To compensate for the differences between the terrain heights used in the regional model and the reanalysis model, the horizontally interpolated soil temperature values are adjusted vertically by assuming a uniform lapse rate of -6.5 K km^{-1} . The spatially and/or temporally varying land surface parameters such as soil texture and monthly green-leaf fraction (GLF) are obtained from Zobler (1986) and Gutman and Iganov (1998), respectively. To be consistent with the assumptions used to retrieve the GLF, the leaf-area index (LAI) is set to a constant value of 4 in the simulation. The vegetation rooting density within the model soil layers is assumed uniform in the horizontal and in the vertical.

3. Precipitation

Figure 2 compares the annual mean precipitation (mm day^{-1}) in the hindcast against 0.5° -resolution analysis by the Climate Research Unit (CRU), University of East Anglia (New et al. 1999, 2000). Important features of precipitation distribution in the CRU data are well simulated in the hindcast. Orographic effects on precipitation in the western United States, such as heavy precipitation over mountain ranges in California (CA), Oregon (OR), Washington (WA), and Idaho (ID), together with the dry regions at the lee side of the Sierra Nevada and the Cascades, appear clearly in the hindcast. Heavy precipitation over the mountain ranges in western Wyoming (WY), central Arizona (AZ) and Utah (UT), and northern New Mexico (NM), which is usually absent in coarse-resolution analyses and GCMs, also appears clearly in the regional simulation. The simulated precipitation, however, shows a systematic bias along the Pacific coast. Precipitation over the Coastal Range in Oregon, Washington, and southern California is underestimated generally, while precipitation over the Cas-

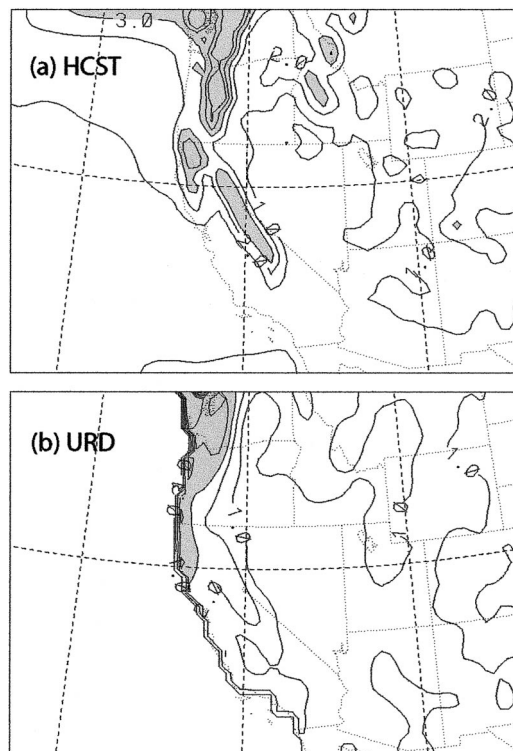


FIG. 2. Annual-mean precipitation (mm day^{-1}) in the (a) hindcast and (b) CRU analysis. The contour levels are 0.1, 1, 2, 3, 4, and 5. Shading indicates the area in which the values exceed 3 mm day^{-1} .

ades and the southern Sierra Nevada is overestimated. A lack of spatial resolution may be the main source of the bias in the simulated spatial distribution along the Pacific coast. The coastal terrain of Oregon, Washington, and southern California is characterized with narrow ridges with steep slopes, and needs a resolution of 10 km or higher (Chung et al. 1998; Kim et al. 2000). Underrepresentation of the coastal terrain underestimates precipitation along the coastal region. This, in turn, results in excessive water vapor flux into the Cascade and the Sierra Nevada, causing the RCM to overestimate precipitation in these high mountain ranges. Note that precipitation in the northern California Coastal Range, which is much wider than that in Oregon, Washington, and southern California, is close to the analysis. The CRU precipitation data in high-elevation regions of the Cascade and the Sierra Nevada may be biased due to a lack of high-elevation rain gauges and smoothing effects of an interpolation scheme used for the analysis (New et al. 2000).

Table 1 compares overland precipitation in the hindcast (MAS), CRU analysis (CRU) and reanalysis (REA). For this comparison, the monthly precipitation values of both analyses are interpolated onto the RCM grid points before they are averaged over the model domain. Compared to the CRU analysis and the reanalysis, the RCM tends to overestimate precipitation in the region, except springtime when the reanalysis precipitation ex-

TABLE 1. The 8-yr average overland precipitation and its spatial standard deviation in the hindcast (MAS), CRU analysis (CRU), and NCEP–NCAR reanalysis (REA). The spatial correlation values are calculated between the simulation and the CRU data (CRU), the simulation and the reanalysis (REA), and the CRU data and the reanalysis (ANL) respectively.

	Mean precipitation (mm month ⁻¹)			Standard deviation (mm month ⁻¹)			Spatial correlation (mm month ⁻¹)		
	MAS	CRU	REA	MAS	CRU	REA	MAS	CRU	REA
Winter (DJF)	59.9	40.8	40.1	72.6	41.3	28.4	0.75	0.73	0.85
Spring (MAM)	44.4	37.4	53.3	32.6	21.2	13.0	0.70	0.57	0.71
Summer (JJA)	42.4	31.7	30.0	35.1	13.0	19.2	0.65	0.65	0.62
Fall (SON)	33.5	30.9	26.6	30.0	24.2	21.4	0.71	0.70	0.83
Whole year	45.1	35.2	37.5	31.6	21.4	15.2	0.71	0.62	0.77

ceeds both the RCM and the CRU data. The overestimation of precipitation in the hindcast is largest (smallest) for the winter (fall). Spatial variations of precipitation, measured by the standard deviation, are also larger in the RCM than both analyses for all seasons. This comparison, however, does not necessarily translate into the absolute bias in RCM precipitation fields. As low-elevation rain gauges outnumber high-elevation ones significantly (New et al. 1999, 2000), the CRU data are biased towards lower-elevation values. The reanalysis precipitation is much smoother than the hindcast due to a coarse resolution of the reanalysis model. Hence, both CRU analysis and reanalysis may have underestimated the spatial variability as well as the total amount of precipitation. The correlation coefficients between the simulated seasonal precipitation and the two analyses range from 0.62 to 0.75. The hindcast precipitation shows higher correlation with the fine-resolution CRU data than the coarse-resolution reanalysis.

For a more quantitative evaluation, we compare the hindcast precipitation against the rain gauge data of the Cooperative Summary of the Day (NCDC 1995, referred to as COOP data hereafter). For this comparison, the RCM data are interpolated onto the locations of individual rain gauges. Then, the interpolated RCM data are spatially (for each state) and temporally (for each month) averaged. To compute monthly values, we use only the gauge data that contains a complete record of daily precipitation for a given month.

Figure 3 compares the seasonal-mean precipitation within eight states from the COOP data (COOP), hindcast, CRU data, and the reanalysis. The hindcast results agree well with the seasonal precipitation variations in the COOP data and CRU analysis. Spatial variations of precipitation such as the winter (summer) maximum (minimum) in the Pacific coast region (CA, OR) and the summer maximum in the regions affected by the North American monsoon are represented clearly in the hindcast. Winter precipitation is somewhat overestimated in Oregon, Idaho, and Nevada. Summer rainfall is overestimated in the interior region (UT, CO) and New Mexico. Relative errors, defined as the difference between the hindcast and the rain gauge data divided by the rain gauge data (see Table 2 for the definition of relative errors), are largest in the interior region, es-

pecially near the eastern boundary of the domain during the summer.

Monthly precipitation (Fig. 4) shows that the winter precipitation errors in Oregon, New Mexico, Idaho, and Nevada in Fig. 3 may not be systematic. For these states, overestimation of precipitation is serious only in the winters of 1993/94 and/or 1994/95. In other periods, the simulated winter precipitation is close to the COOP data. Overestimation of summer rainfall in Colorado appears to be systematic, and is most severe in August. It is suspected that the low-level convergence between the westerly flows and the southeasterly monsoon flows is not handled well in this region as it is too close to the domain boundary. Overestimation of summer rainfall in Utah does not appear to be as systematic as in Colorado. Rainfall errors in Utah may be due to difficulties in correctly simulating convective rainfall.

The annual mean precipitation amount from the COOP data is presented in Fig. 4, together with the temporal correlations and biases in the hindcast and reanalysis precipitation. For the annual mean climatology, the hindcast precipitation agrees closely with the COOP data along the Pacific coast (CA, OR, WA) and in the southwestern United States (AZ, NM), in which the differences between the COOP data and the hindcast are 5%–28%. Correlation coefficients between the hindcast and COOP data range 0.8–0.9. In the interior region, which is strongly affected by summertime convective rainfall, the simulation overestimates the COOP data by 20%–60%. Errors in the hindcast precipitation are especially large in the vicinity of the eastern boundary of the domain, Colorado and Wyoming, where the hindcast overestimates precipitation by as much as 70%. The statewide precipitation from the reanalysis shows similar or better agreement with the COOP data as the hindcast. Even though the reanalysis represents well the temporal variations of the observed precipitation at the scales of individual states, the hindcast captures better the observed spatial variations of precipitation, especially along the Pacific coast and over the regions where precipitation is strongly affected by local terrain. For example, the reanalysis does not capture important features such as heavy precipitation over the Coastal Range, the Cascades, and the Sierra Nevada, and the rain shadow within the Central Valley (Soong and Kim

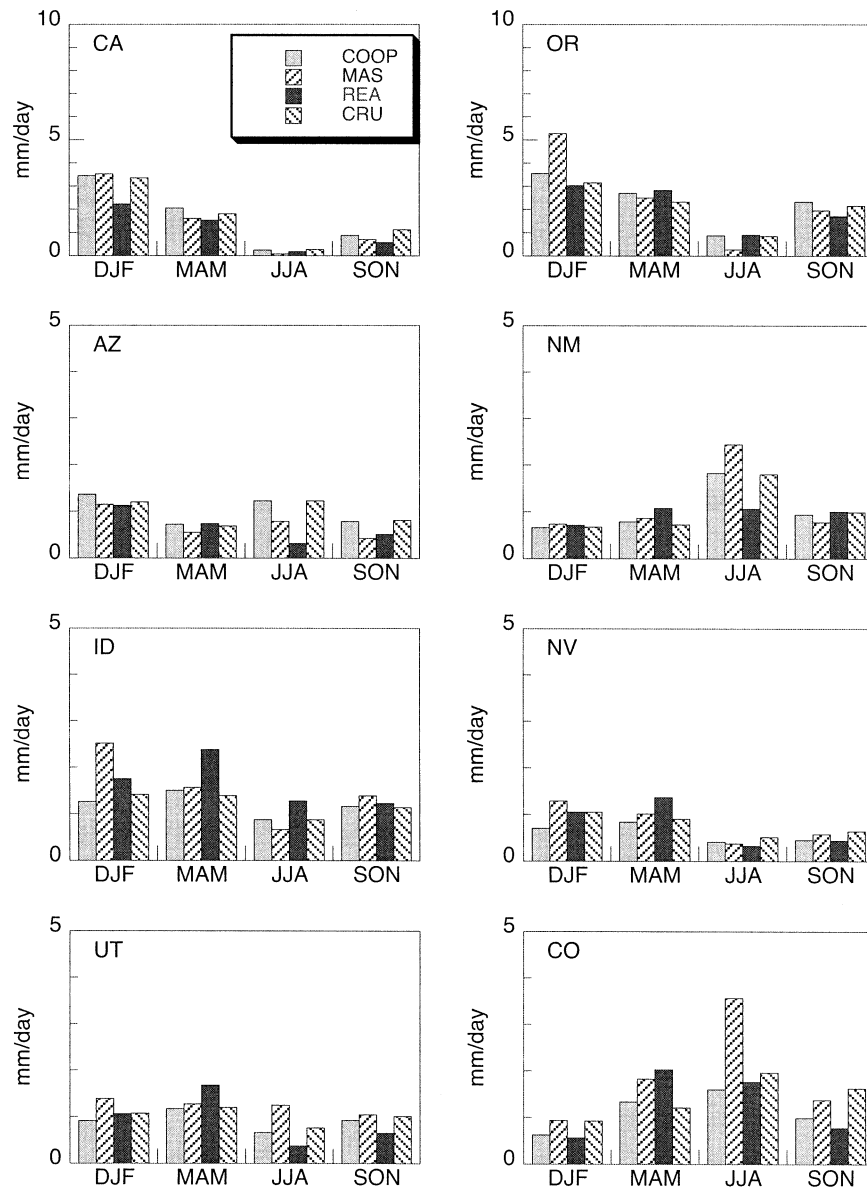


FIG. 3. Seasonal-mean precipitation (mm day^{-1}) for the winter (DJF), spring (MAM), summer (JJA), and fall (SON), from the COOP data (COOP), hindcast (MAS), reanalysis (REA) and CRU (CRU).

1996; Kim 1997). Instead, maximum reanalysis precipitation occurs in the Central Valley (not shown). Other distinct orographic effects, such as precipitation maxima in central Utah and Arizona, are also absent in the reanalysis due to a lack of spatial resolution of the reanalysis model. Such inaccuracies in the reanalysis, mainly due to a coarse spatial resolution of the reanalysis model, are well corrected by the RCM.

To examine the applicability of the RCM data to basin-scale ($100\text{--}1000 \text{ km}^2$) impact assessment studies, the RCM precipitation is compared against rain gauge data, as well as the reanalysis, in four California basins (Fig. 5). The size of each basin ranges from 472 to 886

km^2 , which is similar or smaller than an RCM grid box. The method for computing basin-average values from RCM grid values are presented in Kim et al. (2000). Even though the RCM underestimates (overestimates) precipitation in the coastal (Sierra Nevada) basins, the hindcast results are close to the rain gauge data, especially for the first 6-yr period. During this early period, relative errors of the RCM precipitation are less than 30%, with correlation coefficients of 0.8 or higher. For the entire period, the most notable errors in the simulation appear in January and March 1994, when precipitation in the Sierra Nevada basins (North Fork American, Merced, Carson) is overestimated by as much

TABLE 2. The basin-mean precipitation from the hindcast (MAS) and the reanalysis. The relative error is defined as $\varepsilon \equiv (\bar{P}_{\text{Obs}} - \bar{P}_{\text{Model}}) / \bar{P}_{\text{Obs}}$ where ε is the relative error and the subscript *Model* indicates either the simulation or the reanalysis. Temporal correlation coefficients between the observed and simulated monthly precipitation for each basin are in parentheses.

	Relative errors (1988–92)		Relative error (1988–95)	
	MAS	Reanalysis	MAS	Reanalysis
North Fork	0.08	−0.61	0.38	−0.61
American River	(0.94)	(0.96)	(0.86)	(0.89)
Carson River	0.14	−0.41	0.36	−0.42
	(0.91)	(0.88)	(0.86)	(0.93)
Merced River	0.05	−0.71	0.36	−0.72
	(0.91)	(0.88)	(0.86)	(0.93)

as 100% (Fig. 5). Even though precipitation is also overestimated in this coastal basin (Hopland) for the same period, the error is much smaller than for the Sierra Nevada basins. Unlike the statewide averages, the reanalysis underestimates basin-scale precipitation by over 40% of the rain gauge data for all basins. The reanalysis, however, represents well temporal variations of precipitation (Table 2). Relative errors in reanalysis precipitation remain similar over the entire 8-yr period, while they suddenly increase for the last 1–2 yr of the 8-yr period in the hindcast. The reason for this sudden increase of the RCM precipitation errors during these later years are not clear at this time. Investigations of the simulated large-scale temperature and geopotential height do not indicate any deterioration of the thermodynamic fields compared to the earlier 6-yr period. Despite the errors in the last two winters, the overall performance over the 8-yr period, especially for the first 6 yr, suggests that the RCM-generated precipitation data are more applicable to basin-scale assessments than GCM-generated data.

Interannual variation of the North American monsoon (NAM) leaves distinct signatures in the seasonal precipitation variations in the southwestern United States (Higgins et al. 1999; Kim 2002). Figure 6 presents summer (Fig. 6a) and winter (Fig. 6b) rainfall anomalies in the Arizona–New Mexico region. The RCM precipitation anomalies agree well with both the COOP and the CRU data for both seasons, especially for the winter. The RCM results also show a relationship of dry (wet) summers preceded by wet (dry) winters, one of the distinct features associated with interannual variations of the NAM, for the two wet summers (1988, 1990) and one dry summer (1993) included in the 8-yr period (Higgins et al. 1999; Kim 2002).

Figure 7 presents the frequency of heavy and extreme precipitation events derived from the hindcast and the NCEP Unified Rain gauge Data (URD; Higgins et al. 2000). Following Groisman et al. (2001), the threshold values for the heavy and extreme events are defined as 50.8 and 101.6 mm day^{−1}, respectively. The frequency of heavy precipitation events in the hindcast (Fig. 7a)

agrees well with the one from the URD (Fig. 7c), especially in the northern California Coastal Range, the Cascades, and the Sierra Nevada in which the frequency of the heavy events are highest. The hindcast underestimates the frequency of the heavy events over the Oregon Coastal Range and the southern California Coastal Range, as the RCM resolution is not sufficient to resolve the terrain in these regions (Chung et al. 1998; Kim et al. 2000). The RCM underestimates the frequency of extreme events somewhat (Figs. 7b,d), except in the Cascade and the northern California Coastal Range.

4. Snowfall

The simulated heaviest snowfall occurs in high-elevation areas of the Cascade, the Sierra Nevada, northern California, and the Rocky Mountains (not shown). Strong effects of terrain elevation on snowfall are especially clear in warm and dry southwestern regions (CA, AZ), where the snowfall maxima occur along the ridges of major mountain ranges, with annual mean values exceeding 1000 mm water. In the hindcast, significant snowfall south of 40°N occurs from November to March with a maximum in January. In this region, late winter (February and March) snowfall amount is greater than early winter (November and December) snowfall amount. In the region north of 40°N, the simulated snowfall extends into April, and early winter snowfall amount is about the same as late winter snowfall amount.

Figure 8 compares the monthly mean snowfall in eight states from the Coop data and the hindcast. The simulated monthly snowfall compares well with the station data in all eight states, especially in the interior region (AZ, NM, MT, CO). Snowfall along the Pacific Ocean (CA, NV) is overestimated for the January–March period. Further investigation of the monthly snowfall over the entire 8-yr period (not shown) shows that most of the overestimation in California and Nevada occurs during the 3 months, January–March, of 1994, when large overestimation of precipitation occurs in the same region (Fig. 4). For the first 6 yr (1988–93), snowfall is also overestimated for these two states, but the biases are much smaller than they appear in Fig. 8.

5. Near-surface air temperature

Table 3 shows the 8-yr-mean 2-m air temperature over the land surface in the hindcast and the CRU analysis. Compared to the CRU data, the RCM tends to underestimate seasonal-mean temperature, except for summer. The maximum differences between the hindcast and CRU temperatures appear in winter, when it is as large as 4 K. Spatial variability of the low-level temperature, measured by the standard deviation, is larger in the hindcast than the CRU as well. Despite these differences, the spatial patterns of the low-level temperature in the

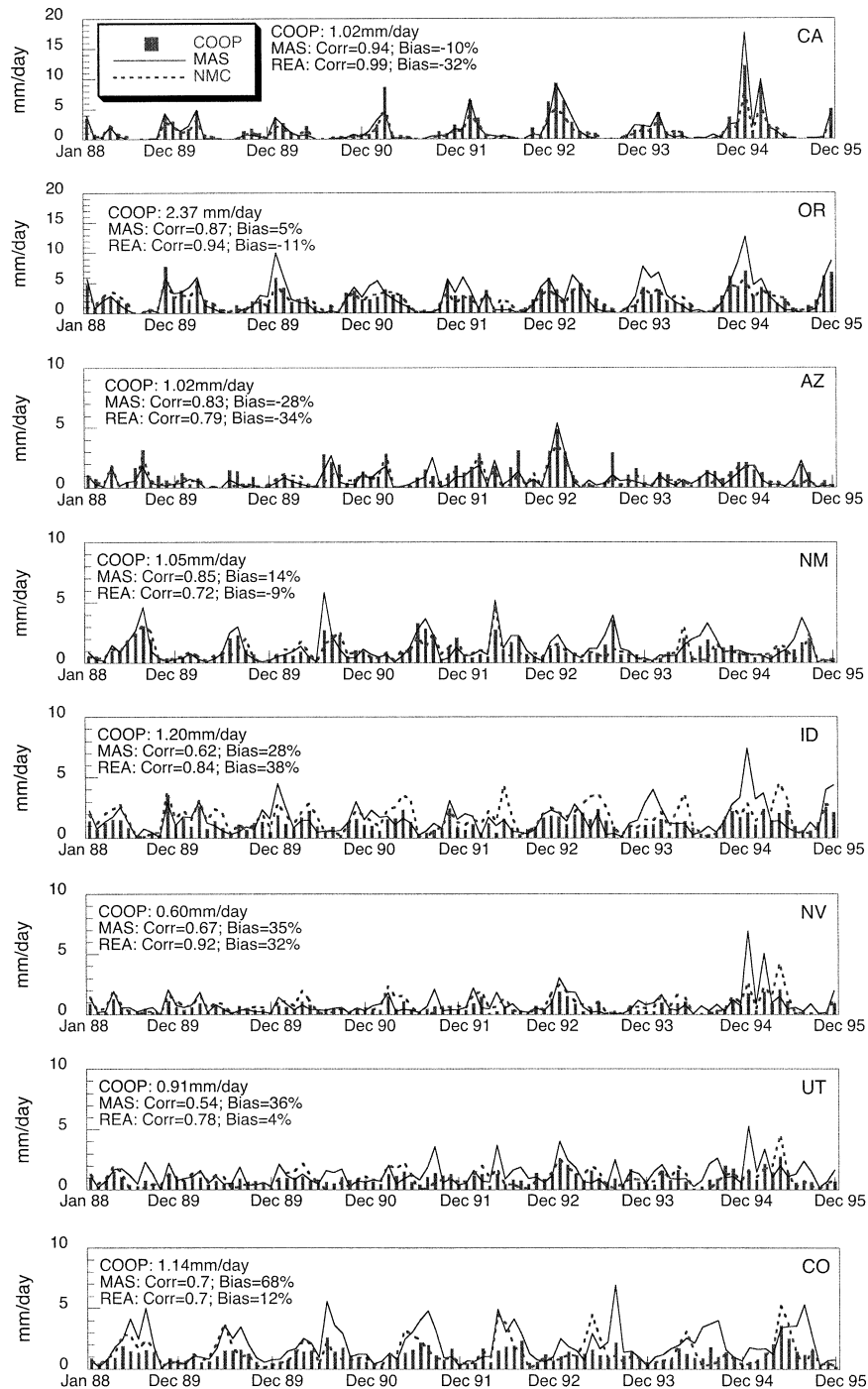


FIG. 4. Statewide monthly precipitation (mm day^{-1}) from the hindcast (MAS), reanalysis (REA), and COOP data (COOP). Abbreviated state names are given in Table 1. The numbers following COOP are the annual mean precipitation amount, Corr is the temporal correlation with the COOP data, and Bias is the relative error with respect to the COOP climatology.

hindcast and CRU analysis are close to each other with correlation coefficients of 0.91–0.95 (Table 3).

The evaluation of the simulated low-level temperature and its spatial variability may be affected by unknown amounts of warm biases in the CRU data. Low-level air

temperatures as well as their spatial variations are affected strongly by the variations in terrain heights. The CRU data do not explicitly account for the effects of terrain elevation, except through the station locations included in the analysis (New et al. 2000). As most

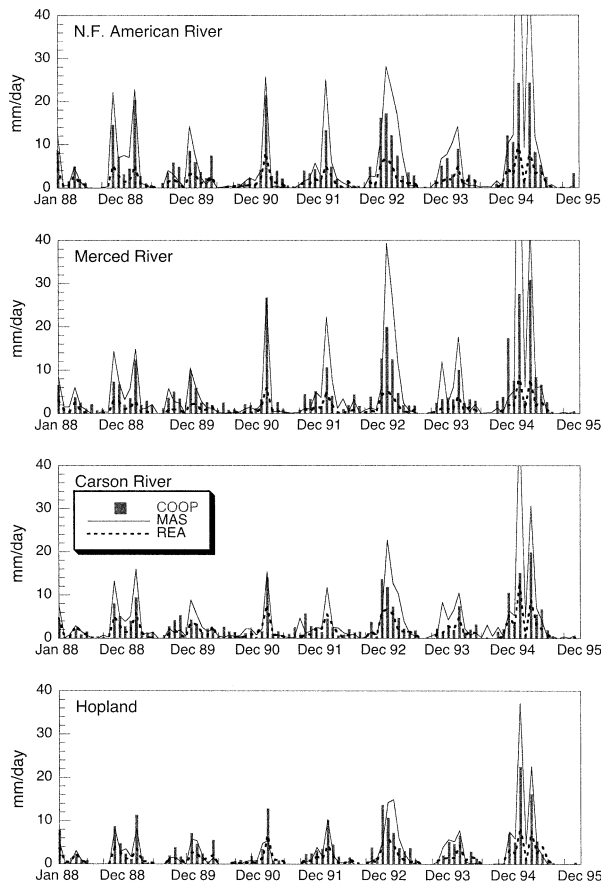


FIG. 5. Monthly precipitation (mm day^{-1}) in four California river basins from the hindcast (MAS), reanalysis (REA), and rain gauge data (COOP).

stations included in the analysis are located in low elevations, the CRU data are biased toward low elevations, causing systematic warm biases in the analyzed temperature field. Hence, the wintertime cold biases may be smaller than the values in Table 3. By the same token, the warm biases in the RCM temperatures during summer may be larger than they appear in Table 3. Note that the warm biases in the CRU data due to underrepresentation of high-elevation stations would be smaller in the summer than the winter, as the low-level lapse rate is generally larger in winter than in summer. In addition, the spatial smoothing associated with the analysis scheme would have further reduced the spatial variability of the analysis output. The effects of the warm biases and smoothing in the CRU analysis are difficult to quantify.

6. Radiation at the surface and top of the atmosphere

The surface insolation (SI) and outgoing longwave radiation at the top of the atmosphere (OLR-TOA) are selected for evaluations. The SI in the reanalysis is

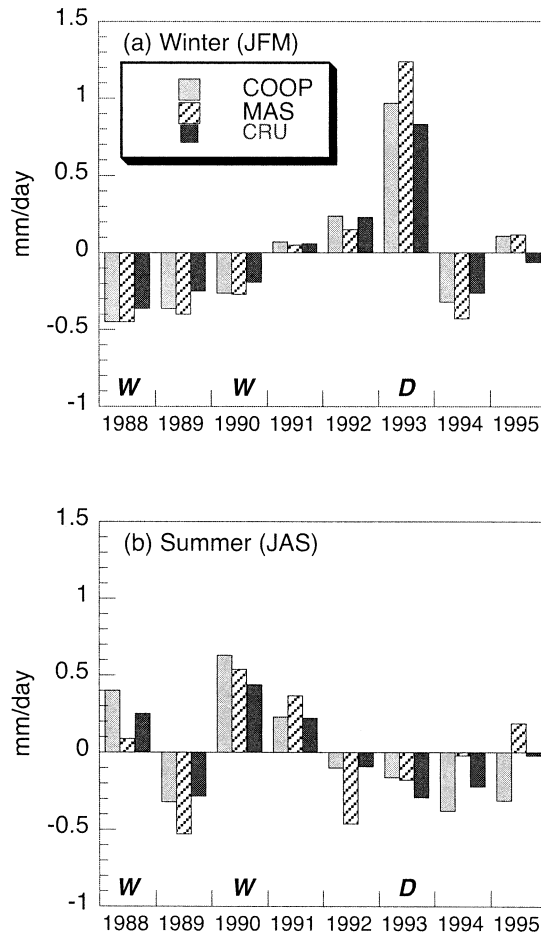


FIG. 6. Interannual variations of the (a) winter and (b) summer precipitation over the AZ-NM region in the hindcast (MAS), COOP data (COOP), and CRU data (CRU).

adopted as a surrogate observation for evaluating the hindcast, as Betts et al. (1996) suggested the SI in the reanalysis is reasonably close to the surface observations. For evaluation of the hindcast OLR-TOA, we employ a long-term 2.5° -resolution analysis of satellite-observed OLR-TOA by Chelliah and Arkin (1992).

Figure 9 compares the monthly mean SI in the hindcast (solid line) against the reanalysis (bars), averaged over the land (Fig. 9a) and the ocean (Fig. 9b). Also shown in Fig. 9 are the relative errors in the simulated SI (dashed line). Note that the relative errors are plotted in upside-down scales. The simulated overland SI agrees closely with the reanalysis, especially for the winter months. Differences between the simulated and reanalysis overland SI are largest in two summer months, June and July, when the relative errors are as large as 10%. The hindcast generally overestimates the over-ocean SI. Relative errors in the simulated over-ocean SI are also largest for June and July. Large errors in the over-ocean SI may be due to underestimation of low-level stratiform clouds in the simulation, which strongly affect the SI over the eastern Pacific. Over-ocean SI errors minimally

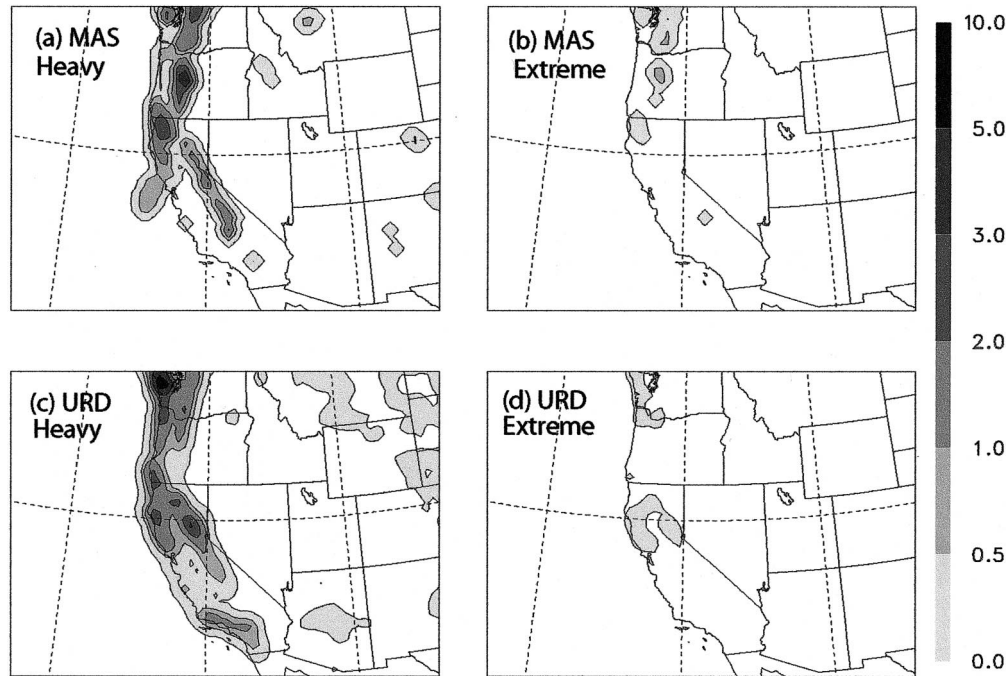


FIG. 7. The frequencies (days yr^{-1}) of heavy and extreme daily precipitation events from the hindcast (MAS) and observations (URD); (a), (c) heavy precipitation frequencies; (b), (d) extreme precipitation frequencies. The observations are inferred from the 0.25° -resolution daily rainfall analysis (URD) by Higgins et al. (2000).

affect the simulation though, as the SST is prescribed over the entire period from the reanalysis.

Figure 10 compares the monthly mean OLR-TOA from the hindcast (solid line) against the satellite data (bars) by Chelliah and Arkin (1992). Like Fig. 9, the relative errors (dashed line) are plotted in upside-down scales. Compared to the satellite data, the hindcast generally overestimates OLR-TOA. Over the land surface (Fig. 10a), both absolute and relative errors are notably larger in summer than winter, suggesting that the RCM overestimates the surface radiative equilibrium temperatures during the summertime. The general overestimation of OLR-TOA also suggests that the cold (warm) biases in the simulated low-level temperature field shown in Table 3, which are estimated against the CRU data, may be smaller (larger) than they appear in Table 3. Over ocean surfaces (Fig. 10b), both absolute and relative errors are slightly larger in winter than summer, even though the interseasonal variations of the relative errors are smaller than over the land.

It is interesting to note that both the hindcast and satellite data show maximum (minimum) OLR-TOA values during the summertime (wintertime) in the western United States, for both land and ocean surfaces. It indicates that the OLR-TOA fields over the western United States as well as over the eastern Pacific included in the domain, are affected mainly by the low tropospheric temperature fields. For this region, summers are characterized by clear skies with low humidity. Even for regions affected by summer monsoon circulation,

mainly Arizona and New Mexico, only a small part of summers is affected by deep convection. As a result, high-level clouds associated with deep convection is not crucial for determining local OLR-TOA fields in the western United States. In contrast, in the regions where high-level clouds associated with deep convections are important (e.g., Tropics, east Asia), minimum (maximum) values of OLR-TOA occur in the summer (winter) season (e.g., Giorgi et al. 1999).

7. Spatial anomaly correlations

Figure 11 presents the spatial anomaly correlations of the monthly mean geopotential height (top) and temperature (bottom) fields between the reanalysis and RCM output at the 500- (dashed) and 300-hPa (solid) levels over the 8-yr period. The lateral boundary nudging area is not included in computing the spatial anomaly correlations. These anomaly correlations show clear seasonal variations, with higher (lower) correlation values during the cold (warm) season. Such a seasonal variation suggests that the effects of the lateral boundary forcing on RCM's interior fields are stronger during the cold season than in the warm season. The anomaly correlations of the 500-hPa (300 hPa) temperature fields stay above 0.9, while those of the 500-hPa (300 hPa) geopotential height fields exceed 0.5 (0.8) during the simulation, except in September 1990. In addition, the differences between the simulated and reanalysis monthly mean values (RCM biases) of temperature and geo-

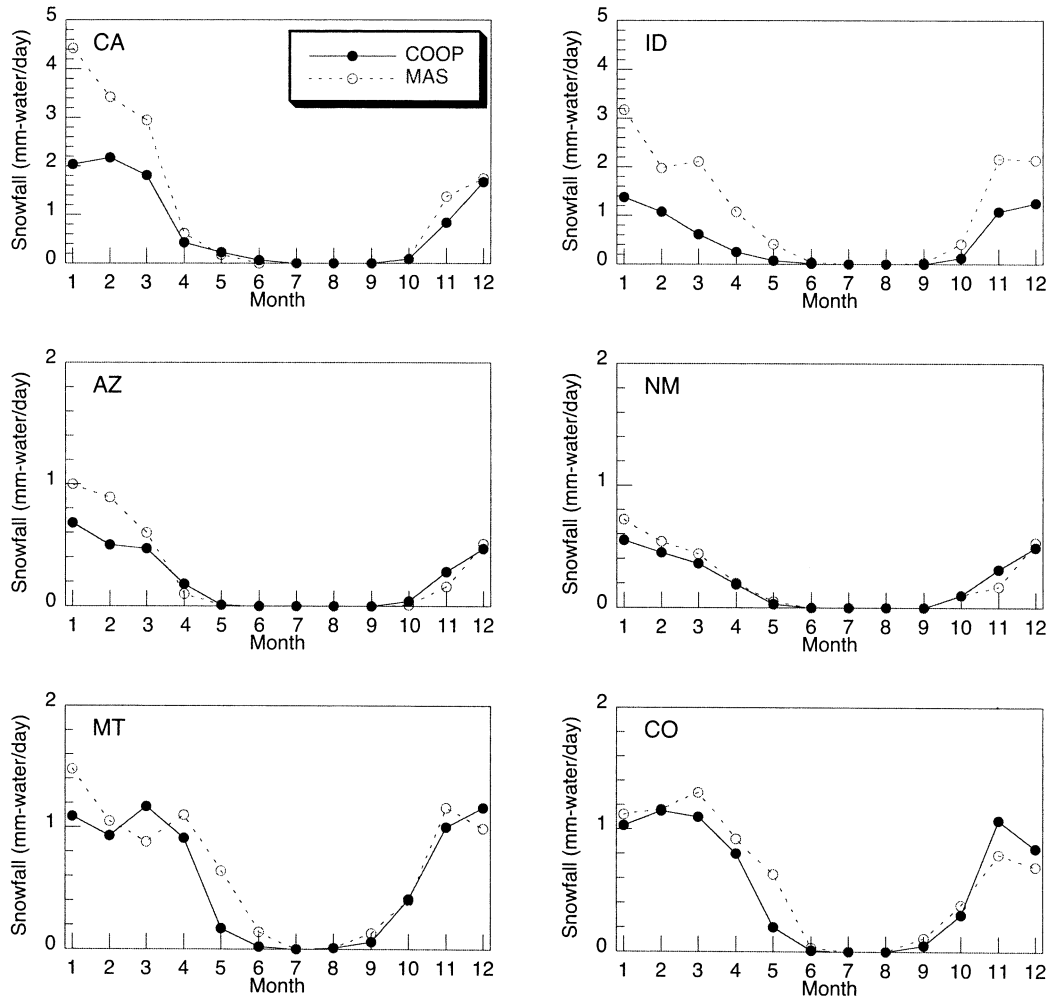


FIG. 8. The observed (COOP) and simulated (MAS) statewide monthly mean snowfall (mm-water day⁻¹) in eight states.

potential height fields are small (less than 1% of the reanalysis values), and remain similar over the entire period (not shown). These temporal variations of the anomaly correlations and the RCM biases suggest that the RCM results do not deteriorate or drift during the 8-yr simulation.

TABLE 3. The seasonal-mean 2-m air temperature and spatial standard deviation over the model domain from the regional climate simulation (MAS) and the CRU climatology.

Season	Mean temperature (°C)		Standard deviation (°C)		Correlation coefficient
	MAS	CRU	MAS	CRU	
Winter (DJF)	-4.3	0.0	6.9	5.7	0.94
Spring (MAM)	6.0	9.4	6.2	4.5	0.94
Summer (JJA)	21.3	20.0	4.4	4.2	0.91
Fall (SON)	9.3	10.6	5.9	4.8	0.95
Whole year	8.0	10.0	5.6	4.6	0.95

8. Summary and discussion

As the first step toward studying the impacts of increased atmospheric CO₂ concentration on the hydrologic cycle and water resources in the western United States, an 8-yr regional climate hindcast was performed using an RCM, the coupled MAS-SPS model. Overall, the RCM simulates the observed characteristics of the regional-scale hydrologic cycle in the region with reasonable accuracy. The spatial and temporal variations of the hindcast precipitation agree closely with observations from rain gauges and analyses. Aggregated at scales of individual states, which are larger than the spatial resolution of the reanalysis model, the simulated precipitation agrees with the CRU analysis with accuracy similar to the reanalysis. The higher RCM resolution, however, yields more accurate basin-scale precipitation than the reanalysis. This improved accuracy in regional-scale precipitation, mainly due to improved representations of terrain height by higher spatial res-

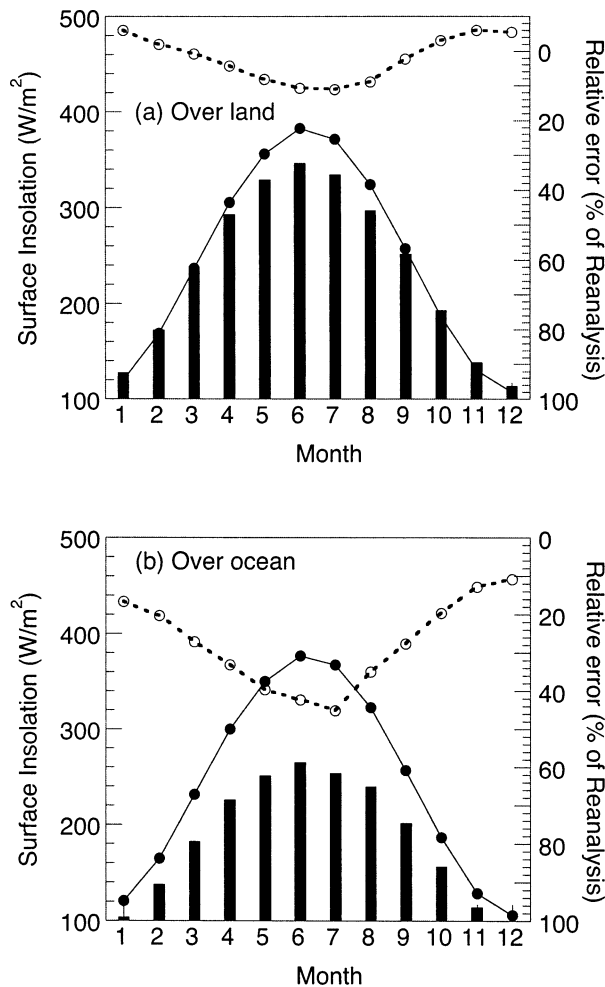


FIG. 9. The simulated (solid line) and observed (bars) monthly mean SI (W m^{-2}) over (a) land and (b) ocean surfaces. The dashed line indicates the relative errors (upside-down scales).

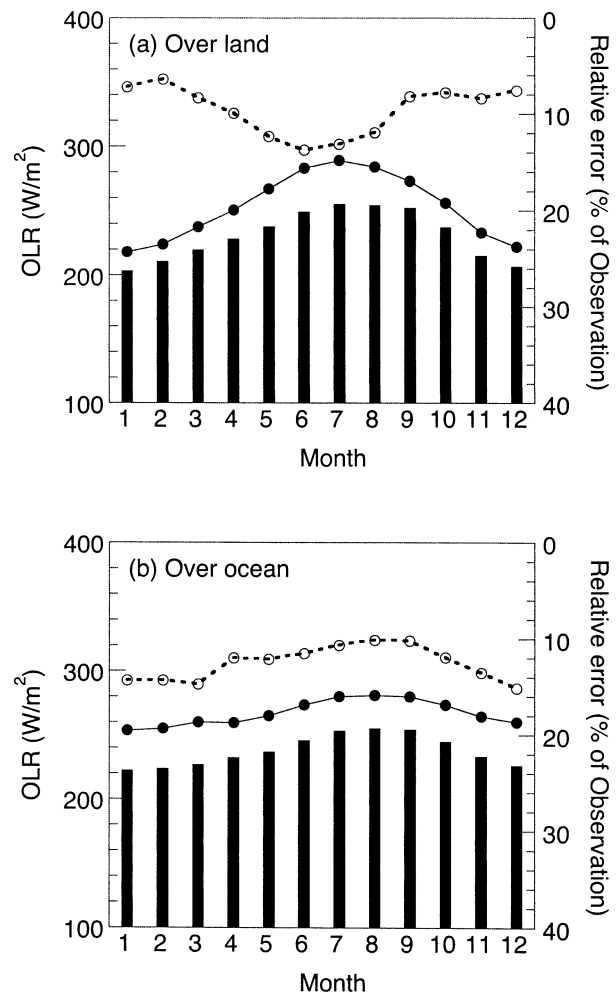


FIG. 10. The simulated (solid line) and satellite-observed (bars) monthly mean OLR-TOA (W m^{-2}) over (a) land and (b) ocean surfaces. The dashed line indicates the relative errors (upside-down scales).

olution, is crucial for studying the impacts of climate change on the hydrologic cycle, extreme events, and water resources in the western United States. The RCM simulates well the frequencies of heavy and extreme precipitation events inferred from a daily rainfall analysis, even though extreme precipitation events are somewhat underestimated. The simulated monthly snowfall agrees with the Coop gauge data with reasonable accuracy, especially in the interior parts of the western United States. Winter precipitation is simulated with higher accuracy than summer rainfall, in general. The most notable errors in the simulated precipitation along the Pacific Ocean appear in the last 2 yr of the hindcast. The errors, however, do not appear to be systematic except in the vicinity of the eastern boundary of the domain.

The simulated low-level air temperature also agrees well with the CRU data, despite general cold biases. The cold biases are largest in high-elevation regions during the cold season. The simulated spatial variability

in the low-level temperature is larger than that obtained from the CRU data as well. The cold biases and overestimation of the spatial variability may not be an accurate measure of RCM errors, however. The station data employed for the CRU analysis are biased towards low elevations due to a lack of high-elevation stations. Hence, the CRU data is expected to be warmer than the true climatology as the low-level air temperature depends strongly on terrain elevation. The smoothing associated with the analysis scheme also tends to reduce the spatial variability. The biases in the CRU climatology are not quantifiable at this time.

Both surface insolation (SI) and OLR-TOA are overestimated compared to the reanalysis and satellite data, respectively. Relative errors in the simulated SI and OLR-TOA are generally larger over the ocean surface than the land surface. The errors in the simulated radiation fields may be associated with underestimation of low-level stratiform clouds over the eastern Pacific

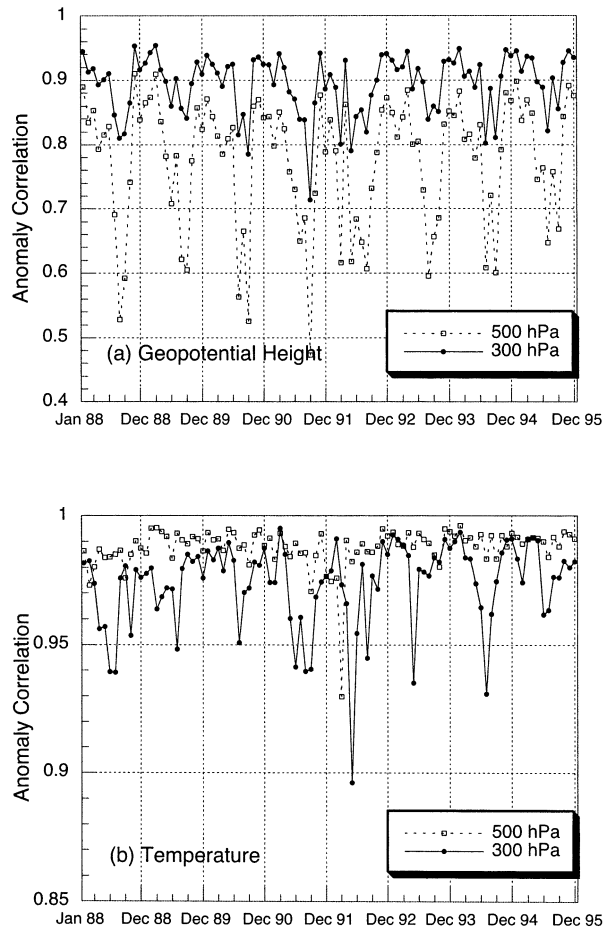


FIG. 11. The spatial anomaly correlations between the simulated and reanalysis monthly mean (a) geopotential heights and (b) temperatures at 500- (dashed) and 300-hPa (solid) levels for the 8-yr period.

as well as the errors in the simulated low-level temperature. Both the hindcast and satellite data suggest that the seasonal variations of OLR-TOA in the western United States are governed primarily by the low-level temperature fields rather than by the high-level clouds due to deep convection. Unlike the regions where deep convection plays an important role in the OLR-TOA fields (e.g., Tropics, east Asia), the maximum (minimum) values of OLR-TOA in the western United States appear in the summer (winter) when near-surface temperature is warm (cold). The means and anomaly correlations of upper-level temperature and geopotential height show that the RCM upper-level fields maintain reasonable agreements with the driving large-scale data over the 8-yr period. It appears that RCM's own drift is negligible, if any, compared to the temporal variability of the large-scale circulation.

Evaluations of the hindcast suggest that the RCM-generated regional-scale fields are reasonably accurate, and preserve the large-scale information of the driving coarse-resolution data well. This refined spatial vari-

ability is crucial for regional climate and climate impact assessment studies, especially in mountainous regions such as the western United States, where the spatial and temporal variations of the hydrologic cycle depend strongly on terrain height.

Acknowledgments. The authors thank Dr. J. D. Farrara for suggestions toward improving the manuscript, and Drs. W. Higgins and W. Shi who made the URD available to us. The CRU analysis and OLR-TOA were obtained from CRU, University of East Anglia, and NOAA, respectively. The Cooperative Summary of Day and the NCEP-NCAR reanalysis were obtained from NOAA-NCDC and the NOAA-CIRES Climate Diagnostics Center, respectively. SDSC and NERSC provided the computational resources. This work was supported by the NASA-MTPE (W-19, 081), NASA-ESE/IDS (NAG5-11363), NASA-RESAC (NS7291), NOAA-PACS (NAOOAANRG0201) and LBNL (LDRD-366139).

REFERENCES

- Barnston, A., A. Leetmaa, V. Kousky, R. Livezey, E. O'Lenic, H. Van den Dool, J. Wagner, and D. Unger, 1999: NCEP forecasts of the El Niño of 1997–98 and its U.S. impacts. *Bull. Amer. Meteor. Soc.*, **80**, 1829–1852.
- Betts, A. K., S.-Y. Hong, and H.-L. Pan, 1996: Comparison of NCEP-NCAR reanalysis with 1987 FIFE data. *Mon. Wea. Rev.*, **124**, 1480–1498.
- Cayan, D. R., L. Riddle, and E. Aguado, 1993: The influence of precipitation and temperature on seasonal streamflow in California. *Water Resour. Res.*, **29**, 1127–1140.
- Chang, S., D. Hahn, C.-H. Yang, D. Norquist, and M. Ek, 1999: Validation study of the CAPS model land surface scheme using the 1987 Cabauw/PILPS dataset. *J. Appl. Meteor.*, **38**, 405–422.
- Chelliah, M., and P. A. Arkin, 1992: Large-scale interannual variability of outgoing longwave radiation anomalies over the global tropics. *J. Climate*, **5**, 371–389.
- Cho, H., M. Niewiadomski, and J. Iribarne, 1989: A model of the effect of cumulus clouds on the redistribution and transformation of pollutants. *J. Geophys. Res.*, **94** (D10), 12 895–12 910.
- Chung, J., J. Kim, J. Oh, and W. Kwon, 1998: Effects of ice-phase physics in simulating grid-scale precipitation. *Kor. J. Atmos. Sci.*, **1**, 94–103.
- Davies, H., 1976: A lateral boundary formulation for multi-level prediction models. *Quart. J. Roy. Meteor. Soc.*, **102**, 404–418.
- Deardorff, J., 1978: Efficient prediction of ground surface temperature and moisture, with inclusion of a layer of vegetation. *J. Geophys. Res.*, **83** (C4), 1889–1903.
- Dickinson, R., R. Errico, F. Giorgi, and A. Bates, 1989: A regional climate model for the western U.S. *Climatic Change*, **15**, 383–422.
- Giorgi, F., and G. Bates, 1989: The climatological skill of a regional model over complex terrain. *Mon. Wea. Rev.*, **117**, 2325–2347.
- , C. Brodeur, and A. Bates, 1994: Regional climate change scenarios over the United States produced with a nested regional climate model. *J. Climate*, **7**, 375–399.
- , J. Hurrell, and M. Marinucci, 1997: Elevation dependency of the surface climate change signal: A model study. *J. Climate*, **10**, 288–296.
- , Y. Huang, K. Nishizawa, and C. Fu, 1999: A seasonal cycle simulation over eastern Asia and its sensitivity to radiative transfer and surface processes. *J. Geophys. Res.*, **104** (D6), 6403–6423.

- Goodridge, J. D., 1994: A study of 1000 year storms in California. Preprints, *Predicting Heavy Rainfall Events in California: A Symposium to Share Weather Pattern Knowledge*, Rocklin, CA, Sierra College, 3–72.
- Groisman, P. Ya., R. W. Knight, and T. R. Karl, 2001: Heavy precipitation and high streamflow in the contiguous United States: Trends in the twentieth century. *Bull. Amer. Meteor. Soc.*, **82**, 219–246.
- Gutman, G., and A. Iganov, 1998: Derivation of green vegetation fraction from NOAA VHRR for use in numerical weather prediction models. *Int. J. Remote Sens.*, **19**, 1533–1543.
- Harshvardhan, D. Randall, and T. Corsetti, 1987: A fast radiation parameterization for atmospheric circulation models. *J. Geophys. Res.*, **92** (D1), 1009–1016.
- Higgins, R. W., Y. Chen, and A. V. Douglas, 1999: Interannual variability of the North American warm season precipitation regime. *J. Climate*, **12**, 653–680.
- , W. Shi, E. Yarosh, and R. Joyce, cited 2000: *Improved United States Precipitation Quality Control and Analysis*. Atlas No. 7, NCEP/Climate Prediction Center. [Available online at http://www.cpc.ncep.noaa.gov/research_papers/ncep_cpc_atlas/7/index.html.]
- Hong, S.-Y., and H.-L. Pan, 1998: Convective trigger function for a mass flux cumulus parameterization scheme. *Mon. Wea. Rev.*, **126**, 2599–2620.
- , and A. Leetmaa, 1999: An evaluation of the NCEP RSM for regional climate modeling. *J. Climate*, **12**, 592–609.
- Kalnay, E., and Coauthors, 1996: The NCEP/NCAR 40-Year Reanalysis Project. *Bull. Amer. Meteor. Soc.*, **77**, 437–471.
- Kim, J., 1997: Precipitation and snow budget over the southwestern United States during the 1994–1995 winter season in a mesoscale model simulation. *Water Resour. Res.*, **33**, 2831–2839.
- , 2001: A nested modeling study of elevation-dependent climate change signals in California induced by increased atmospheric CO₂. *Geophys. Res. Lett.*, **28**, 2951–2954.
- , 2002: Precipitation variability associated with the North American Monsoon in the 20th century. *Geophys. Res. Lett.*, **29**, 1650, doi:10.1029/2001GL014316.
- , and L. Mahrt, 1992: Simple formulation of turbulent mixing in a stable free atmosphere and nocturnal boundary layer. *Tellus*, **44A**, 381–394.
- , and M. Ek, 1995: A simulation of the surface energy budget and soil water content over the Hydrologic Atmospheric Pilot Experiments-Modelisation du Bilan Hydrique forest site. *J. Geophys. Res.*, **100** (D10), 20 845–20 854.
- , and S.-T. Soong, 1996: Simulation of a precipitation event in the western United States. *Regional Impacts of Global Climate Change*, S. Ghan et al., Eds., Battelle Press, 73–84.
- , N. L. Miller, A. K. Guetter, and K. P. Georgakakos, 1998a: River flow response to precipitation and snow budget in California during the 1994–1995 winter. *J. Climate*, **11**, 2376–2386.
- , ———, J. Oh, J. Chung, and D. Rha, 1998b: Eastern Asian hydrometeorology simulation using the Regional Climate System Model. *Global Planet. Change*, **19**, 225–240.
- , ———, J. D. Farrara, and S.-Y. Hong, 2000: A numerical study of precipitation and streamflow in the western United States during the 1997/98 winter season. *J. Hydrometeor.*, **1**, 311–329.
- , T. Kim, R. W. Arritt, and N. L. Miller, 2002: Impacts of increased atmospheric CO₂ on the hydroclimate of the western United States. *J. Climate*, **15**, 1926–1942.
- Louis, J. F., M. Tiedke, and J. Gelvyn, 1982: A short history of the operational PBL-parameterization at ECMWF. *Proc. Workshop on Planetary Boundary Layer Parameterization*, Reading, United Kingdom, ECMWF, 59–79. [Available from ECMWF, Shinfield Park, Reading, RG 29AX, United Kingdom.]
- Mahrt, L., and H.-L. Pan, 1984: A two-layer model of soil hydrology. *Bound.-Layer Meteor.*, **29**, 1–20.
- Mearns, L. O., C. Rosenzweig, and R. Goldberg, 1996: The effects of changes in daily and interannual climatic variability on CERES-WHEAT—A sensitivity study. *Climatic Change*, **32**, 257–292.
- NCDC, 1995: *Cooperative Summary of the Day*. CD-ROM set, NCDC. [Available from NCDC Federal Bldg., 151 Patton Ave., Asheville, NC 28801.]
- New, M., M. Hulme, and P. Jones, 1999: Representing twentieth-century space–time climate variability. Part I: Development of a 1961–90 mean monthly terrestrial climatology. *J. Climate*, **12**, 829–856.
- , ———, and ———, 2000: Representing twentieth-century space–time climate variability. Part II: Development of 1901–96 monthly grids of terrestrial surface climate. *J. Climate*, **13**, 2217–2238.
- Pan, H.-L., and L. Mahrt, 1987: Interaction between soil hydrology and boundary layer development. *Bound.-Layer Meteor.*, **38**, 185–202.
- , and W. Wu, 1995: Implementing a mass flux convection parameterization package for the NCEP medium-range forecast model. NMC Office Note, 40 pp. [Available from NCEP/EMC, 5200 Auth Road, Camp Springs, MD 20764.]
- Soong, S.-T., and J. Kim, 1996: Simulation of a heavy precipitation event in California. *Climatic Change*, **32**, 55–77.
- Starr, D., and S. Cox, 1985: Cirrus clouds. Part I: A cirrus cloud model. *J. Atmos. Sci.*, **42**, 2663–2681.
- Stephens, G., 1978: Radiation profiles in extended water clouds. II: Parameterization schemes. *J. Atmos. Sci.*, **35**, 2123–2132.
- Takacs, L., 1985: A two-step scheme for the advection equation with minimized dissipation and dispersion errors. *Mon. Wea. Rev.*, **113**, 1050–1065.
- Zobler, L., 1986: A world soil file for global climate modeling. NASA Tech. Memo. 87802, 33 pp.